COMPDYN 2013
4th ECCOMAS Thematic Conference on
Computational Methods in Structural Dynamics and Earthquake Engineering
M. Papadrakakis, V. Papadopoulos, V. Plevris (eds.)
Kos Island, Greece, 12–14 June 2013

A THREE DIMENSIONAL MULTISCALE FORMULATION FOR THE NONLINEAR DYNAMIC ANALYSIS OF MASONRY STRUCTURES

Savvas P. Triantafyllou[1], **Eleni N. Chatzi**[2]

Institute of Structural Engineering
ETH Zürich
Wolfgang-Pauli-Strasse 15
CH-8093 Zürich, Switzerland
e-mail: [1]triantafyllou.ibk.baug.ethz.ch, [2]chatzi.ibk.baug.ethz.ch

Keywords: Composites, Multiscale, Hysteretic, Masonry.

Abstract. *In this work, a three dimensional multiscale formulation is presented for the analysis of masonry structures based on the multiscale finite element formulation. The method is develloped within the framework of the Enhanced Multiscale Finite Element Method. Through this approach, two discretization schemes are considered, namely a fine mesh that accounts for the micro-structure and a coarse mesh that encapsulates the former. Through a numerically derived mapping, the fine scale information is propagated to the coarse mesh where the numerical solution of the governing equations is performed. Inelasticity is introduced at the fine mesh by considering a set of internal variables corresponding to the plastic deformation accumulatimg at the Gauss points of each fine-scale element. These additional quantities evolve according to properly defined smooth evolution equations. The proposed formalism results in a nonlinear dynamic analysis method where the micro-level state matrices need only be evaluated once at the beginning of the analysis procedure. The accuracy and computational efficiency of the proposed scheme is verified through an illustrative example.*

1 INTRODUCTION

Composite materials consist of two or more mechanically separable solid materials. As such, they in general exhibit a heterogeneous micro-structure whose specific morphology affects the mechanical behavior of the assembled structure [19]. Composites are therefore multiscale in nature, i.e. the scale of the constituents is of lower order than the scale of the resulting material. Furthermore, the resulting structure, that is an assemblage of composites, can be of an even larger scale than the scale of the constituents e.g. a textile strengthened masonry structure [14] or a bio-sensor consisting of several nano-wires [23]. Thus, the required modeling approach has to account for such a level of detailing that spreads through scales of significantly different magnitude. Throughout this paper, the term macroscopic (or coarse) scale corresponds to the structural level whereas the term microscopic (or fine) scale corresponds to the composite micro-structure properties such as the sizes, morphologies and distributions of heterogeneities that the material consists of.

Modeling of structures that consist of composites could be accomplished using the standard finite element method [35]. However, a finite element model mesh accounting for each micro-structural heterogeneity would require large amounts of computer memory and CPU time. Therefore, the finite element scheme is usually restricted to small scale numerical experiments of a representative volume element (RVE) [21, 28]. To properly capture the effect of micro-structural heterogeneities in the large scale, more refined methods have been developed. Instead of implementing the finite element method as is, upscaled or multiscale methods exist that account for such types of problems.

Multiscale methods can be separated in two groups, namely multiscale homogenization methods [24] and multiscale finite element methods (MsFEMs) [12]. Within the framework of the averaging theory for ordinary and partial differential equations, multiscale homogenization methods are based on the evaluation of an averaged strain and corresponding stress tensor over a predefined space domain denoted as Representative Volume (RVE). Amongst the various homogenization methods proposed [15], asymptotic homogenization has been proven to be very efficient both in terms of accuracy and required computational cost [7, 33]. However, homogenization methods rely on two basic assumptions, namely the full separation of the individual scales and the local periodicity of the RVEs. In practice, the heterogeneities within a composite are not periodic as in the case of fiber-reinforced matrices. In order to adapt to general heterogeneous materials, the size of the RVE must be sufficiently large to contain enough microscopic heterogeneous information [29, 16] which results in a considerable increase of the computational cost. Furthermore, in an elasto-plastic problem, periodicity on the RVEs also dictates periodicity on the damage induced which could result in erroneous results.

The multiscale finite element method, instead, relies on the numerical evaluation of a set of micro-scale basis functions that are used to map the micro-structure information onto the larger scale. These basis functions depend on the micro-structural geometry and constituent material properties. MsFEM was first introduced in [18] although a variant of the method was earlier introduced in the pioneering work of [5] for one-dimensional problems and later improved to account for higher order elements [4, 3]. Although MsFEMs have been extensively used in linear and nonlinear flow simulation analysis [12, 16] the method has not been implemented in structural mechanics problems. This is attributed to the inherent inability of the method to treat the bulk expansion/ contraction phenomena (i.e. Poissons effect). To overcome this problem, the enhanced multiscale finite element method (EMsFEM) has been proposed for the analysis of heterogeneous structures [34]. EMsFEM introduces additional coupling terms into the

fine-scale interpolation functions to consider the coupling effect among different directions in multi-dimensional vector problems. However, in a nonlinear analysis procedure, the numerical basis functions need to be evaluated at every incremental step due to the progressive failure of the constituents thus diminishing the computational advantage of the method. The problem is treated in [34] through the implementation of the the initial stiffness method [25] for the solution of the incremental governing equations. Nevertheless, this method is known to face serious convergence problems and usually requires a large number of iterations to achieve convergence [25]. The computational cost increases in a nonlinear dynamic analysis scheme, where a time integration scheme is also needed on top of the iterative procedure [17].

In this work, a modified multiscale finite element analysis procedure is presented for the nonlinear static and dynamic analysis of heterogeneous structures. In this, the evaluation of the micro-scale basis functions is accomplished within the hysteretic finite element framework [30]. Inelasticity is treated at the element level through properly defined evolution equations that control the evolution of the plastic part of the deformation component. Using the Principle of Virtual Work, the tangent stiffness matrix of the element is replaced by an elastic stiffness matrix and a hysteretic stiffness matrix that both remain constant throughout the analysis. A multiaxial smooth hysteretic model is implemented to control the evolution of the plastic strains. This model is derived on the basis of the Bouc-Wen model of hysteresis [8] and accounts for any kind of yield criterion and hardening law within the framework of classical plasticity [20]. Smooth hysteretic modelling has proven very efficient with respect to classical incremental plasticity in computationally intense problems such as nonlinear structural identi-fication [9] and stochastic dynamics [27, 32]. Furthermore, the proposed hysteretic scheme can be extended to account for cyclic damage induced phenomena such as stiffness degradation and strength deterioration [13].

2 HYSTERETIC MODELING

2.1 Multiaxial modelling of hysteresis

The material model implemented in this work is a generic rate-independent hysteretic model. This model accounts for any type of yield criterion and hardening law either isotropic, kinematic or combined. Both the case of linear and nonlinear kinematic hardening is considered.

The model is defined on the grounds of two rate equations. The first equation controls the evolution of the stress field with respect to the strain field and assumes the following form

$$\{\dot{\sigma}\} = [D]\left([I] - H_1 H_2 [R]\right)\{\dot{\varepsilon}\} \tag{1}$$

where $\{\sigma\}$ is the stress tensor, $[D]$ is the elastic constitutive matrix, $[I]$ is the identity matrix while $(\cdot)$ denotes differentiation with respect to time while H_1 and H_2 are smoothened Heaviside functions that will be defined later on. Matrix $[R]$ in equation (1) is a strain interaction matrix defined through the following relation

$$[R] = \{\alpha\}\left(-\{b\}^T \mathscr{G}\left(\{\eta\}, \Phi\right) + (\alpha)^T [D]\{\alpha\}\right)\{\alpha\}^T [D] \tag{2}$$

where $\{\alpha\} = \left(\partial\Phi/\partial\{\sigma\}\right)^T$, $\{b\} = \left(\partial\Phi/\partial\{\eta\}\right)^T$ and $\mathscr{G}\left(\{\eta\}, \Phi\right)$ is a hardening function corresponding to the kinematic hardening rule considered.

The second equation of the constitutive model used in this work defines the evolution of the back-stress with respect to the strain field and assumes the following form:

$$\{\dot{\eta}\} = H_1 H_2 \mathscr{G}\left(\{\eta\}, \Phi\right)\left[\tilde{R}\right]\{\dot{\varepsilon}\} \tag{3}$$

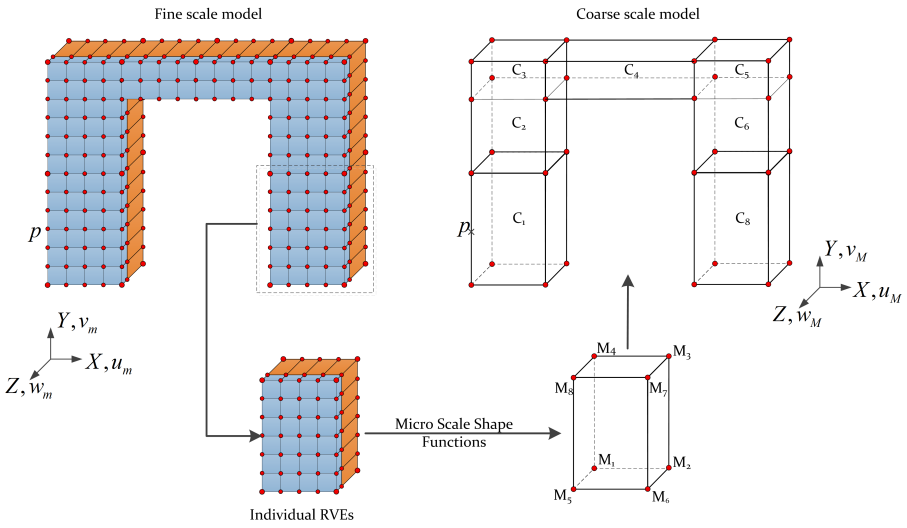

Figure 1: Multiscale Finite Element procedure

where $\left[\tilde{R}\right]$ is the corresponding hardening interaction matrix defined by the following relation

$$\left[\tilde{R}\right] = \left(-\{b\}^T \mathscr{G}\left(\{\eta\}, \Phi\right) + \{\alpha\}^T [D] \{\alpha\}\right)^{-1} \{\alpha\}^T [D] \tag{4}$$

The smoothed Heaviside functions H_1 and H_2introduced in relations (1) and (3) assume the following form, namely

$$H_1 = \left|\frac{\Phi\left(\{\sigma\}, \{\eta\}\right)}{\Phi_0}\right|^N, \quad N \geq 2 \tag{5}$$

and

$$H_2 = \beta + \gamma sgn\left(\{\varepsilon\}^T \{\dot{\sigma}\}\right) \tag{6}$$

where $\Phi = \Phi\left(\{\sigma\}, \{\eta\}\right)$ is a yield criterion, Φ_0 the yield limit,N a material parameter that determines the rate at which the yield criterion reaches its maximum value while β and γ are material parameters that control the stiffness at the moment of unloading.

3 THE MULTISCALE FINITE ELEMENT ANALYSIS METHOD

In this Section, the Enhanced Multiscale Finite Element Method (EMsFEM) is briefly discussed as a reference for subsequent derivations. A masonry frame is presented in Figure 1, consisting of two piers and a horizontal spandrel. An additional outer layer of reinforcement is also considered. The computational fine scale model consists of 8-node hex elements [35]. Instead of directly solving the fine scale computational model using the standard isoparametric finite element formulation, EMsFEM is based on a two-step approach. Grouping together clusters of micro-elements, a set of coarse elements is constructed. The nodes of the derived macro-elements are the macro-nodes of the coarse mesh. Accordingly, two displacement fields are defined, namely the micro-displacement field corresponding to the micro nodal displacements $\left\{ \begin{array}{ccc} u_m(x,y) & v_m(x,y) & w_m(x,y) \end{array} \right\}^T$ of the fine mesh and the macro-displacement field $\left\{ \begin{array}{ccc} u_M(x,y) & v_M(x,y) & w_M(x,y) \end{array} \right\}^T$ corresponding to the macro nodal displacements. Throughout this work, subscript m denotes a micro-measure while M is used to denote a macro-measure of the indexed quantity.

Next, a numerical mapping is constructed that maps the micro-displacement field within each RVE to the corresponding macro-displacements of the RVE macro-nodes. This numerical mapping assumes the following generic form:

$$\{d\}_m = \mathscr{M}\{d\}_M \tag{7}$$

where $\mathscr{M}$ is a mapping operator. EMsFEM is based on the assumption that the discrete micro-displacements within the coarse element are interpolated at the macro-nodes using the following scheme:

$$\begin{array}{l} u_m(x_j,y_j) = \sum_{i=1}^{n_{Macro}} N_{ijxx}u_{M_i} + \sum_{i=1}^{n_{Macro}} N_{ijxy}v_{M_i} + \sum_{i=1}^{n_{Macro}} N_{ijxz}w_{M_i} \\ v_m(x_j,y_j) = \sum_{i=1}^{n_{Macro}} N_{ijxy}u_{M_i} + \sum_{i=1}^{n_{Macro}} N_{ijyy}v_{M_i} + \sum_{i=1}^{n_{Macro}} N_{ijyz}w_{M_i} \quad j = 1...n_{micro} \\ w_m(x_j,y_j) = \sum_{i=1}^{n_{Macro}} N_{ijxz}u_{M_i} + \sum_{i=1}^{n_{Macro}} N_{ijyz}v_{M_i} + \sum_{i=1}^{n_{Macro}} N_{ijzz}w_{M_i} \end{array} \tag{8}$$

where u_m, v_m, w_m are the horizontal and vertical micro-displacement components, n_{Macro} is the number of macro-nodes of the coarse element, (x_j, y_j, z_j) are the local coordinates of the micro-nodes, u_{M_i}, v_{M_i}, w_M are the horizontal and vertical displacement components of the macro-nodes, N_{ixx}, N_{ixy}, N_{iyy}, N_{iyz}, N_{izz} are the micro-basis functions and n_{micro} is the number of micro-nodes within the coarse element.

In equation (8), N_{ijxx} stands for the displacement component of node j along the x axis induced by a unilateral displacement at the i node (also along the x axis). Likewise, N_{ijxy} stands for the displacement component of the i node, along the x axis induced by a unilateral displacement at node j and along the y axis. Contrary to MsFEM where the interpolation fields of the displacement components are considered uncoupled, the coupling terms N_{ixy}, N_{ixz}, N_{iyz} are introduced in EMsFEM. Thus, equation (8) results in a kinematical assumption consistent with the observation that a unit displacement in the boundary of a deformable body may induce displacements in both directions within the body.

From the interpolation field introduced in equation (8), the following relation can be established at the micro-elemental level

$$\{d\}_{m(i)} = [N]_{m(i)}\{d\}_M \tag{9}$$

where $\{d\}_{m(i)}$ is the nodal displacement vector of the i_{th} micro-element, $[N]_{m(i)}$ is a matrix containing the micro-basis shape functions evaluated at the nodes of the i_{th} micro-element while $\{d\}_M$ the vector of nodal displacements of the corresponding macro-nodes.

3.1 Numerical evaluation of micro-scale basis functions

The evaluation of the mapping operator $\mathscr{M}$ is performed numerically. Relation (8) successfully maps the micro-displacement field to the macro-displacement field if and only if the micro-shape functions adhere to the following property, namely, when the macro-displacement component is equal to unity at a macro-node, displacement is equal to zero at every other macro-node. The derivation of micro-basis functions with such properties can be accomplished by considering the following boundary value problem

$$\begin{array}{l} [K]_{RVE}\{d\}_m = \{\emptyset\} \\ \{d\}_S = \{\bar{d}\} \end{array} \tag{10}$$

where $[K]_{RVE}$ is the stiffness matrix of the RVE, $\{\emptyset\}$ is a vector containing zeros while $\{d\}_S$ is a vector containing the nodal degrees of freedom of the boundary S of the RVE and $\{\bar{d}\}$ is a

vector of prescribed displacements. The RVE stiffness matrix is formulated using the standard finite element method [8]. In this work, the solution of the boundary value problem established in equation (10) is performed using the Lagrange multiplier method [6].

The choice of the values of the prescribed boundary displacements is a key assumption of the EMsFEM and highly affects the accuracy of the derived multiscale scheme. Three different types of boundary conditions are established in the literature namely linear boundary conditions, periodic boundary conditions and oscillatory boundary conditions with oversampling. Further details on the procedure implemented for the derivation of the micro-basis functions can be found in [12].

4 THE PROPOSED NUMERICAL SCHEME

The evaluation of the micro-shape functions for each RVE is based on the solution of the equilibrium problem (10). Thus, the mapping depends on the material properties of the fine-scale model, e.g. for the case of the reinforced masonry RVE presented in Figure 1, the solution depends on the material properties of masonry and the composite matrix. Consequently, in a nonlinear analysis procedure, either static or dynamic, the evaluation of the micro to macro-mapping needs to be performed in every incremental step of the analysis procedure. To overcome this computational drawback, the hysteretic formulation of finite elements is implemented [30] in this work to account for the fine scale nonlinear material behaviour.

Considering the additive decomposition of the strain rate into a reversible elastic an an irreversible plastic part [22] within the micro-element, the following relation is established:

$$\left\{\dot{\varepsilon}\right\}_{m(i)} = \left\{\dot{\varepsilon}^{el}\right\}_{m(i)} + \left\{\dot{\varepsilon}^{pl}\right\}_{m(i)} \tag{11}$$

where $\{\varepsilon\}_{m(i)}$ is the tensor of total micro-strain within the i_{th} micro-element, $\left\{\varepsilon^{el}\right\}_{m(i)}$ is the tensor of the elastic strain, $\left\{\varepsilon^{pl}\right\}_{m(i)}$ is the tensor of the inelastic, irreversible strain while $(.)$ denotes differentiation with respect to time. The vectorial notation of the stress and strain tensors is used in this work. Using equation (11) the elastic Hooke's stress-strain law is cast into the following form

$$\left\{\dot{\sigma}\right\}_{m(i)} = \left[D\right]_{m(i)} \left\{\dot{\varepsilon}^{el}\right\}_{m(i)} = \left[D\right]_{m(i)} \left(\left\{\dot{\varepsilon}\right\}_{m(i)} - \left\{\dot{\varepsilon}^{pl}\right\}_{m(i)}\right) \tag{12}$$

where $\{\sigma\}$ is the stress tensor and $\left[D\right]_{m}$ is the elastic material constitutive matrix [11] of the micro-element. Comparing equations (1) and (12) the following expression for the evolution of the plastic strain component is readily derived:

$$\left\{\dot{\varepsilon}^{pl}\right\}_{m(i)} = H_1 H_2 \left[R\right]_{m(i)} \left\{\dot{\varepsilon}\right\}_{m(i)} \tag{13}$$

where the interaction matrix $\left[R\right]_{m(i)}$ is introduced in equation (2). The following rate form of the principle of virtual displacements is introduced [31] over the finite volume V_e of a single element:

$$\int_{V_e} \left\{\varepsilon\right\}_{m(i)}^{T} \left\{\dot{\sigma}\right\}_{m(i)} dV_e = \left\{d\right\}_{m(i)}^{T} \left\{\dot{f}\right\}_{m(i)} \tag{14}$$

where $\left\{d\right\}_{m(i)}$ is the vector of micro-nodal displacements introduced in relation (9) and $\left\{f\right\}_{m(i)}$ is the corresponding vector of nodal forces. For the sake of the presentation, only nodal loads are considered herein, however the evaluation of body loads and surface tractions can be derived

accordingly. Substituting equation (12) into the variational principle (14) the following relation is derived:

$$\int_{V_e} \{\varepsilon\}^T_{m(i)} [D]_{m(i)} \{\dot{\varepsilon}\}_{m(i)} dV_e - \int_{V_e} \{\varepsilon\}^T_{m(i)} [D]_{m(i)} \left\{\dot{\varepsilon}^{pl}\right\}_{m(i)} dV_e = \{d\}^T_{m(i)} \left\{\dot{f}\right\}_{m(i)} \quad (15)$$

Considering the standard isoparametric interpolation scheme [35] for the micro-displacement field $\{u\}_{m(i)}$

$$\{u\}_{m(i)} = [N]_{m(i)} \{d\}_{m(i)} \quad (16)$$

with the accompanying strain-displacement compatibility relation:

$$\{\varepsilon\}_{m(i)} = [B]_{m(i)} \{d\}_{m(i)} \quad (17)$$

where $[N]_{m(i)}$ is the matrix of shape functions for the 8-node solid element [35], and $[B]_{m(i)} = \partial [N]_{m(i)}$ is the corresponding strain-displacement matrix. Substituting equation (17) into equation (15) the following relation is derived:

$$\int_{V_e} [B]^T_{m(i)} [D]_{m(i)} [B]_{m(i)} dV_e \left\{\dot{d}\right\}_{m(i)} - \int_{V_e} [B]^T_{m(i)} [D]_{m(i)} \left\{\dot{\varepsilon}^{pl}\right\}_{m(i)} dV_e = \left\{\dot{f}\right\}_{m(i)} \quad (18)$$

Furthermore, introducing an interpolation scheme for the plastic part of the strain $\left\{\varepsilon^{pl}\right\}_{m(i)}$, namely:

$$\left\{\dot{\varepsilon}^{pl}\right\}_{m(i)} = [N]_{em(i)} \left\{\dot{\varepsilon}^{pl}_{cq}\right\}_{m(i)} \quad (19)$$

where $\left\{\varepsilon^{pl}_{cq}\right\}_{m(i)}$ is the vector of plastic stains retrieved at properly defined collocation points, the following relation is finally derived:

$$\left[k^{el}\right]_{m(i)} \left\{\dot{d}\right\}_{m(i)} - \left[k^{h}\right]_{m(i)} \left\{\dot{\varepsilon}^{pl}_{cq}\right\}_{m(i)} = \left\{\dot{P}\right\}_{m(i)} \quad (20)$$

where $\left[k^{el}\right]_{m(i)}$ is the elastic stiffness matrix of the micro-element

$$\left[k^{el}\right]_{m(i)} = \int_{V_e} [B]^T_{m(i)} [D]_{m(i)} [B]_{m(i)} dV_e \quad (21)$$

and $\left[k^{h}\right]_{m(i)}$ is the hysteretic matrix of the micro-element.

$$\left[k^{h}\right]_{m(i)} = \int_{V_e} [B]^T_{m(i)} [D]_{m(i)} [N]_{em(i)} dV_e \quad (22)$$

Both $\left[k^{el}\right]_{m(i)}$ and $\left[k^{h}\right]_{m(i)}$ are constant and inelasticity is controlled at the collocation points through the accompanying plastic strain evolution equations defined in equation (13).

Considering zero initial conditions for brevity, rates in equation (20) are dropped and the following relation is established

$$\left[k^{el}\right]_{m(i)} \{d\}_{m(i)} - \left[k^{h}\right]_{m(i)} \left\{\varepsilon^{pl}_{cq}\right\}_{(i)} = \{f\}_{m(i)} \quad (23)$$

Substituting equation (9) into equation (23) and pre-multiplying with $[N]^T_{m(i)}$ the following relation is derived:

$$\left[k^{el}\right]^M_{m(i)} \{d\}_M - \left[k^{h}\right]^M_{m(i)} \left\{\varepsilon^{pl}_{cq}\right\}_{(i)} = \{f\}^M_{m(i)} \quad (24)$$

where

$$\left[k^{el}\right]^{M}_{m(i)} = [N]^{T}_{m(i)} \left[k^{el}\right]_{m(i)} [N]_{m(i)} \tag{25}$$

is the elastic stiffness matrix of the i_{th} micro-element mapped onto the macro-element degrees of freedom while $\left[k^{h}\right]^{M}_{m(i)}$ is the hysteretic matrix of the i_{th} micro-element, evaluated by the following relation:

$$\left[k^{h}\right]^{M}_{m(i)} = [N]^{T}_{m(i)} \left[k^{h}\right]_{m(i)} \tag{26}$$

Finally, $\{P\}^{M}_{m(i)}$ in equation (24) is the equivalent nodal force vector of the micro-element mapped onto the macro-nodes of the coarse element.

$$\{f\}^{M}_{m(i)} = [N]^{T}_{m(i)} \{f\}_{m(i)} \tag{27}$$

Equation (24) is a multiscale equilibrium equation involving the displacement vector evaluated at the coarse-element nodes and the plastic part of the strain tensor evaluated at collocation points within the micro-scale element mesh.

4.1 Micro to Macro scale transition

Having established the micro-element equilibrium in terms of macro-displacement measures using the micro-basis mapping introduced in equation (9), a procedure is needed to formulate the global equilibrium equations in terms of the macro-quantities. Denoting with a subscript M the corresponding macro-measures over the volume V of the coarse element equation (14) is re-written as:

$$\int_{V_M} \{\varepsilon\}^{T}_{M} \{\dot{\sigma}\}_{M} \, dV_M = \{d\}^{T}_{M} \left\{\dot{f}\right\}_{M} \tag{28}$$

where $\{f\}_{M}$ is the vector of nodal loads imposed at the coarse element nodes. Equivalently to relation (20) the variation principle of equation (28) gives rise to the following equation:

$$\int_{V_M} \{\varepsilon\}^{T}_{M} \{\dot{\sigma}\}_{M} \, dV_M = [K]^{M}_{CR(j)} \left\{\dot{d}\right\}_{M} - \left[K^{h}\right]^{M}_{CR(j)} \left\{\dot{\varepsilon}^{pl}_{cq}\right\}_{M} \tag{29}$$

where $[K]^{M}_{CR(j)}$, $\left[K^{h}\right]^{M}_{CR(j)}$ are the equivalent stiffness matrix and the equivalent hysteretic matrix of the j_{th} coarse element respectively. These matrices need to be expressed in terms of micro-scale measures, to account for the micro-scale effect upon the macro-scale mesh. This is accomplished by demanding that the strain energy of the coarse element is additively decomposed into the contributions of each micro-element within the coarse-element. Thus, the following relation is established:

$$\int_{V} \{\varepsilon\}^{T}_{M} \{\sigma\}_{M} \, dV = \sum_{i=1}^{m_{el}} \int_{V_{mi}} \{\varepsilon\}^{T}_{mi} \{\sigma\}_{mi} \, dV_i \tag{30}$$

where $\{\varepsilon\}_{mi}$, $\{\sigma\}_{mi}$ are the micro-strain and micro-stress field defined over the volume V_{mi} of the i_{th} micro-element. Using relations and (14) (15), the following relation is established for the r.h.s of equation (30)

$$\sum_{i=1}^{m_{el}} \int_{V_{mi}} \{\varepsilon\}^{T}_{mi} \{\sigma\}_{mi} \, dV_i = \sum_{i=1}^{m_{el}} \left(\{d\}^{T}_{mi} \left[k^{el}\right]_{m(i)} \{d\}_{m(i)} - \{d\}^{T}_{mi} \left[k^{h}\right]_{m(i)} \left\{\varepsilon^{pl}_{cq}\right\}_{m(i)} \right) \tag{31}$$

Substituting relation (24) into relation (31), the following relation is derived

$$\sum_{i=1}^{m_{el}} \int_{V_{mi}} \{\varepsilon\}_{mi}^{T} \{\sigma\}_{mi} \, dV_i = \{d\}_M^T \sum_{i=1}^{m_{el}} \left([N]_{Mi}^T \left[k^{el}\right]_{m(i)} [N]_{Mi} \{d\}_M - [N]_{Mi}^T \left[k^h\right]_{m(i)} \left\{\varepsilon_{cq}^{pl}\right\}_{m(i)} \right) \tag{32}$$

Using equations (29) and (32), equation (30) assumes the following form:

$$[K]_{CR(j)}^M \{d\}_M - \left[K^h\right]_{CR(j)}^M \left\{\varepsilon^{pl}\right\}_{cq} = \sum_{i=1}^{m_{el}} \left[k^{el}\right]_{m(i)}^M \{d\}_M - \sum_{i=1}^{m_{el}} \left[k^h\right]_{m(i)}^M \left\{\varepsilon_{cq}^{pl}\right\}_{m(i)} \tag{33}$$

Relation (33) holds for every compatible vector of nodal displacements $\{d\}_M$ as long as:

$$[K]_{CR(j)}^M = \sum_{i=1}^{m_{el}} \left[k^{el}\right]_{m(i)}^M \tag{34}$$

and

$$\left[K^h\right]_{CR(j)}^M \left\{\varepsilon_{cq}^{pl}\right\} = \sum_{i=1}^{m_{el}} \left[k^h\right]_{m(i)}^M \left\{\varepsilon_{cq}^{pl}\right\}_{m(i)} \tag{35}$$

thus, the following multiscale equilibrium equation is derived for the coarse element:

$$[K]_{CR(j)}^M \{d\}_M = \{f\}_M - \{f_h\}_M \tag{36}$$

where $\{f_h\}_M$ is a nonlinear correction to the external force vector arising from the evolution of the plastic strains within the micro-structure

$$\{f_h\}_M = \sum_{i=1}^{m_{el}} \left[k^h\right]_{m(i)}^M \left\{\varepsilon_{cq}^{pl}\right\}_{m(i)} \tag{37}$$

while the plastic strain vectors $\left\{\varepsilon_{cq}^{pl}\right\}_{m(i)}$ are considered to evolve according to relation (13). Equations (36) and (37) are used to derive the equilibrium equation at the structural level.

4.2 Solution in the macro-scale

Considering the general case of a coarse mesh with $ndof_M$ free macro-degrees of freedom and using equation (36), the global equilibrium equations of the composite structure can be established in the coarse mesh. In the dynamic case the following equation is established:

$$[M] \left\{\ddot{U}\right\}_M + [C] \left\{\dot{U}\right\}_M + [K] \{U\}_M = \{F\}_M + \{F_h\}_M \tag{38}$$

where $[M]$, $[C]$, $[K]$ are the $(ndof_M \times ndof_M)$ macro-scale mass, viscous damping and stiffness matrix respectively. The mass matrix can be formulated following either the lamped or distributed mass approach while the viscous damping can be of either the classical or non-classical type [10]. The global stiffness matrix of the composite structure is formulated through the direct stiffness method by additively appending the contributions of the coarse elements equivalent matrices defined in equation (34). The $(ndof_M \times 1)$ vector $\{U\}_M$ consists of the nodal macro-displacements.

Equation (36) expresses the nodal equilibrium of the coarse element mesh. The coarse element equivalent stiffness matrices $[K]_{CR(j)}^M$ can be assembled through the direct stiffness

method to derive the stiffness matrix of the composite structure. The external load vector $\{F\}_M$ and the hysteretic load vector $\{F_h\}_M$ are assembled considering the equilibrium of the corresponding elemental contributions $\{f\}_M$ and $\{f_h\}_M$, defined in equations (28) and (37) respectively, at coarse nodal points.

Equations (38) are supplemented by the evolution equations of the micro-plastic strain components defined at the collocation points within the micro-elements. These equations can be established in the following form:

$$\left\{\dot{E}^{pl}_{cq}\right\}_m = [G]\left\{\dot{\varepsilon}_{cq}\right\}_m \tag{39}$$

where the vector

$$\left\{\dot{E}^{pl}_{cq}\right\}_m = \left\{ \begin{array}{cccc} \left\{\dot{\varepsilon}^{pl}_{cq}\right\}_{m(1)} & \left\{\dot{\varepsilon}^{pl}_{cq}\right\}_{m(2)} & \cdots & \left\{\dot{\varepsilon}^{pl}_{cq}\right\}_{m(m_{el})} \end{array} \right\}^T \tag{40}$$

holds the plastic strain components evaluated at the collocation points of its micro-element and

$$\left\{\dot{E}_{cq}\right\}_m = \left\{ \begin{array}{cccc} \left\{\dot{\varepsilon}_{cq}\right\}_{m(1)} & \left\{\dot{\varepsilon}_{cq}\right\}_{m(2)} & \cdots & \left\{\dot{\varepsilon}_{cq}\right\}_{m(m_{el})} \end{array} \right\}^T \tag{41}$$

Matrix $[G]$ in relation (39) is a band diagonal matrix that assumes the following form

$$[G] = \left[\begin{array}{ccc} H_{1m(1)}H_{2m(1)}\left[R\right]_{m(1)} & & [0] \\ & H_{1m(2)}H_{2m(2)}\left[R\right]_{m(2)} & \\ [0] & & \ddots \\ & & H_{1m(m_{el})}H_{2m(m_{el})}\left[R\right]_{m(m_{el})} \end{array} \right] \tag{42}$$

Equations (39) are independent and thus can be solved in the micro-element level resulting in an implicitly parallel scheme. Relation (42) depends on the current micro-stress state within each micro-element. The corresponding stress tensors are evaluated from the current micro-strains, using equations (16) and (17).

5 EXAMPLE

In this example a benchmark problem is examined for the verification of the proposed method. The simplified masonry wall presented in Figure 2(a) is considered, consisting of stone blocks and bonding mortar. Furthermore, an outer layer of textile component reinforcement is considered. The stone and mortar material properties (Table 2) are derived from [26]. A J_2 plasticity model is assumed for the stone layer while a Mohr-Coulomb yield criterion is considered for the mortar [2]. For the purpose of this example, homogenized material properties are considered for the textile composite layer [14] whose behaviour is assumed to be elastic until failure. The corresponding anisotropic properties are presented in Table 1.

Two analysis models are considered, namely a fine meshed Finite Element model (FE) and a multiscale model. The FE model is analysed using the Abaqus commercial code [1]. The FEM model is meshed with 2280 hex elements(Figure 2(b)). The second model consists of a single coarse hex element, with the corresponding micro-structure being identical to the FE model. The micro-basis shape functions are evaluated considering periodic boundary conditions at the boundary surfaces of the coarse element. An average acceleration Newmark scheme is implemented for the solution of the governing equations of motion with a constant time step

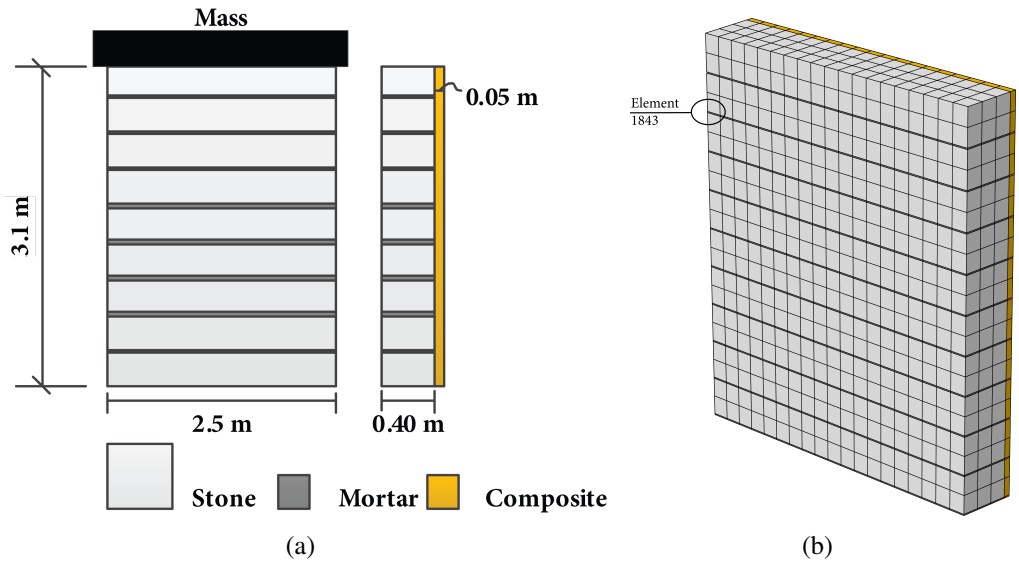

(a) (b)

Figure 2: (a) Textile composite reinforced stone masonry wall (b) Fem hex-mesh

	Mortar	**Stone**
Young's modulus [MPa]	3494	20200
Poisson's ratio	0.11	0.2
Plasticity	Mohr-Coulomb	von-Mises
Friction angle [deg]	21.8	-
Cohesion [MPa]	0.1	-
Yield Stress [MPa]	-	69.2

Table 1: Masonry wall: Constituent Properties

Young's modulus [MPa]	$E_{11} = 54000$	$E_{22} = 53200$	$E_{33} = 53200$
	$E_{12} = 53200$	$E_{23} = 54000$	$E_{23} = 54000$
Poisson's ratio	$\nu_{12} = 0.14$	$\nu_{23} = 0.2$	$\nu_{13} = 0.2$

Table 2: Textile Reinforcement Material Properties

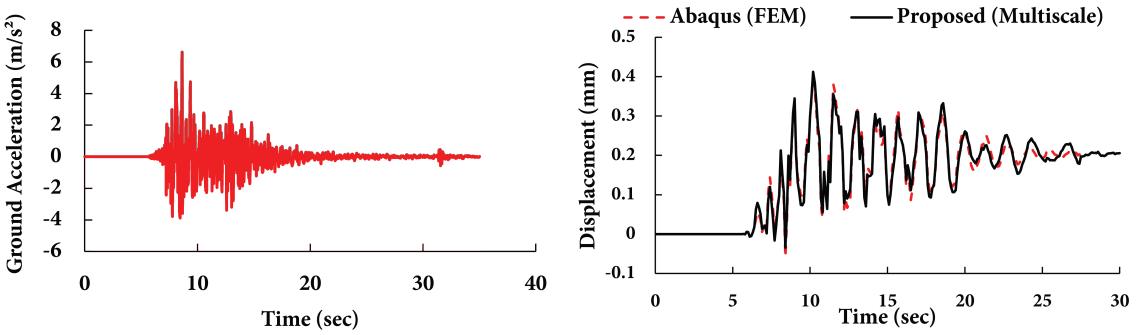

(a) (b)

Figure 3: (a) V. A. Centro Valle ground acceleration record (L' Aquila, 2009) (b) Top layer horizontal displacement time history

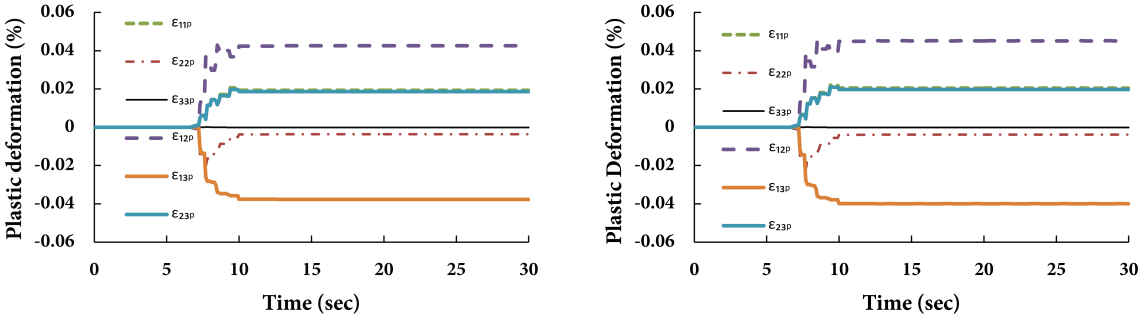

(a) (b)

Figure 4: (a) FEM (b) Proposed Method

equal to $dt = 0.01sec$. Viscous damping is not taken into account in this example. Material nonlinearity in Abaqus is treated through a Full Newton scheme.

An additional mass of 400 KN is considered at the top of the wall. The structure is subjected to the L' Aquila ground motion record presented in Figure 3(a) with a peak acceleration equal to $a_{max} = 0.66g$ In Figure 3(a) the horizontal relative displacement time history at the top layer of the masonry is presented as derived from the two different analysis schemes.

The results obtained from the two different methodologies are in good agreement. The differences observed, especially in the low frequency oscillations near the end of the analysis, are attributed to the numerical assumptions governing the evaluation of the effective stiffness of the coarse element. The gradual shift of the horizontal displacement is a result of plastic deformation accumulating at the mortar joints. In Figure 4 the evolution of the plastic strain components evaluated at the mortar element -1843- (Figure 2(b)) are presented as derived from Abaqus (Figure 4(a)) and the proposed formulation (Figure 4(b))) respectively.

The evolution of the plastic strain components is practically identical in both methods. However, the values predicted in the multiscale model are slightly larger, in agreement with the displacement time-history presented in Figure 3(b).

6 CONCLUSIONS

In this work, a novel multiscale finite element formulation is presented for the nonlinear analysis of masonry structures. The method is based on the Enhanced Multiscale Finite Element Method and the hysteretic formulation of Finite Elements. A set of smoothly evolving inelastic quantities is considered in the fine scale that accounts for the plastic part of the deformation component. Implementing the EMsFEM micro to macro-mapping for the micro displacement components the motion equations of the structure are formulated in the macro-scale. The plastic deformation evolution equations are also transferred into the coarse scale governing equations. Thus, a multiscale formulation is derived where the state matrices, namely the coarse scale stiffness matrix and the fine scale hysteretic matrix are evaluated only once at the beginning of the analysis and remain constant throughout the solution process. The validity of the proposed method is verified through a benchmark test, simulating the dynamic response of a single wall element under earthquake load.

REFERENCES

[1] RI. Abaqus version 6.11 [Computer software]. Dassault Systmes Simulia, Providence.

[2] A. H. Akhaveissy. Limit state strength of unreinforced masonry structures. *Earthquake Spectra*, 29(1):1–31, 2013.

[3] I. Babuška and U. Banerjee. Stable generalized finite element method (sgfem). *Computer Methods in Applied Mechanics and Engineering*, 201204:91 – 111, 2012.

[4] I. Babuška, G. Caloz, and J. Osborn. Special finite element methods for a class of second order elliptic problems with rough coefficients. *SIAM Journal on Numerical Analysis*, 31(4):945–981, 1994.

[5] I. Babuška and J. E. Osborn. Generalized finite element methods: Their performance and their relation to mixed methods. *SIAM Journal on Numerical Analysis*, 20(3):pp. 510–536, 1983.

[6] T. Belytschko, Y. Y. Lu, and L. Gu. Element-free galerkin methods. *International Journal for Numerical Methods in Engineering*, 37(2):229–256, 1994.

[7] A. Bensoussan, J. L. Lions, and G. Papanicolaou. *Asymptotic Analysis for Periodic Structures*. North Holland, Amsterdam, 1978.

[8] R. Bouc. Forced vibration of mechanical systems with hysteresis. In *Proceedings of the Fourth Conference on Non-linear oscillation, Prague, Czechoslovakia*, 1967.

[9] Eleni N. Chatzi, Andrew W. Smyth, and Sami F. Masri. Experimental application of on-line parametric identification for nonlinear hysteretic systems with model uncertainty. *Structural Safety*, 32(5):326 – 337, 2010.

[10] A. Chopra. *Dynamics of Structures*. Prentice Hall, New York, 2006.

[11] E.P. J. Den Hartog. *Strength of Materials*. Dover, New York, 1999.

[12] Y. Efendiev and T. Y. Hou. *Multiscale Finite Element Methods*, volume 4 of *Surveys and Tutorials in the Applied Mathematical Sciences*. Springer, 2009.

[13] S. Erlicher and O. Bursi. Boucwen-type models with stiffness degradation: Thermodynamic analysis and applications. *Journal of Engineering Mechanics*, 134(10):843–855, 2008.

[14] C. Fuggini, E. Chatzi, and D. Zangani. Combining genetic algorithms with a meso-scale approach for system identification of a smart polymeric textile. *Computer-Aided Civil and Infrastructure Engineering*, 28(3):227–245, 2013.

[15] M. G. D. Geers, V. G. Kouznetsova, and W. A. M. Brekelmans. Multi-scale computational homogenization: Trends and challenges. *Journal of Computational and Applied Mathematics*, 234(7):2175–2182, 2010.

[16] Xinguang He and Li Ren. Finite volume multiscale finite element method for solving the groundwater flow problems in heterogeneous porous media. *Water Resources Research*, 41(10):n/a–n/a, 2005.

[17] Hans M. Hilber, Thomas J. R. Hughes, and Robert L. Taylor. Improved numerical dissipation for time integration algorithms in structural dynamics. *Earthquake Engineering & Structural Dynamics*, 5(3):283–292, 1977.

[18] Thomas Y. Hou and Xiao-Hui Wu. A multiscale finite element method for elliptic problems in composite materials and porous media. *Journal of Computational Physics*, 134(1):169 – 189, 1997.

[19] A.K. Kaw. *Mechanics of Composite Materials*. CRC Press, second edition, 1997.

[20] J. Lubliner. *Plasticity Theory*. Dover Publications, New York, 2008.

[21] M.R. Nedele and M.R. Wisnom. Finite element micromechanical modelling of a unidirectional composite subjected to axial shear loading. *Composites*, 25(4):263 – 272, 1994.

[22] S. Nemat-Naser. On finite deformation elasto-plasticity. *International Journal of Solids and Structures*, 18(10):857–872, 1982.

[23] Harold S. Park. A multiscale finite element method for the dynamic analysis of surface-dominated nanomaterials. *International Journal for Numerical Methods in Engineering*, 83(8-9):1237–1254, 2010.

[24] G. A. Pavliotis and A. M. Stuart. *Multiscale Methods, Averaging and Homogenization*. Texts in Applied Mathematics. Springer, Berlin, 2008.

[25] Graham Powell and Jeffrey Simons. Improved iteration strategy for nonlinear structures. *International Journal for Numerical Methods in Engineering*, 17(10):1455–1467, 1981.

[26] R. Senthivel and P.B. Loureno. Finite element modelling of deformation characteristics of historical stone masonry shear walls. *Engineering Structures*, 31(9):1930 – 1943, 2009.

[27] P. D. Spanos and I. A. Kougioumtzoglou. Harmonic wavelet-based statistical linearization of the bouc-wen hysteretic model. pages 2649–2656. Taylor and Francis Group, 2011.

[28] A. Taliercio. Macroscopic strength estimates for metal matrix composites embedding a ductile interphase. *International Journal of Solids and Structures*, 44(22-23):7213–7238, 2007.

[29] K. Terada, M. Hori, T. Kyoya, and N. Kikuchi. Simulation of the multi-scale convergence in computational homogenization approaches. *International Journal of Solids and Structures*, 37(16):2285–2311, 2000.

[30] S. P. Triantafyllou and V. K. Koumousis. A hysteretic quadrilateral plane stress element. 82(10-11):1675–1687, 2012.

[31] K Washizu. *Variational Methods in Elasticity and Plasticity*. Pergamon Press, Oxford, 1983.

[32] K. Worden and J. J. Hensman. Parameter estimation and model selection for a class of hysteretic systems using bayesian inference. *Mechanical Systems and Signal Processing*, 32:153–169, 2012.

[33] Q. Yu and J. Fish. Multiscale asymptotic homogenization for multiphysics problems with multiple spatial and temporal scales: A coupled thermo-viscoelastic example problem. *International Journal of Solids and Structures*, 39(26):6429–6452, 2002.

[34] H. W. Zhang, J. K. Wu, and J. Lv. A new multiscale computational method for elasto-plastic analysis of heterogeneous materials. *Computational Mechanics*, 49(2):149–169, 2012.

[35] O. C. Zienkiewicz, R. L. Taylor, and J.Z. Zhu. *The Finite Element Method: Its Basis and Fundamentals*. Elsevier, Amsterdam, 6 edition, 2005.